Journal of ELECTRONIC MATERIALS, Vol. 47, No. 1, 2018
DOI: 10.1007/s11664-017-5810-4

Strong Visible Light Photocatalytic Activity of Magnetically Recyclable Sol–Gel-Synthesized $ZnFe_2O_4$ for Rhodamine B Degradation

XIAOLI XU,[1] LINGBO XIAO,[1] YANMIN JIA,[1,3] YUANTIGN HONG,[1] JIANGPING MA,[1] and ZHENG WU[2,4]

1.—Department of Physics, Zhejiang Normal University, Jinhua 321004, People's Republic of China. 2.—College of Geography and Environmental Sciences, Zhejiang Normal University, Jinhua 321004, People's Republic of China. 3.—e-mail: ymjia@zjnu.edu.cn. 4.—e-mail: wuzheng@zjnu.edu.cn

Visible light-responsive $ZnFe_2O_4$ photocatalyst with a spinel structure was synthesized via a sol-gel method. The visible light photocatalysis of $ZnFe_2O_4$ was investigated by decomposing Rhodamine B (RhB) solution. Under ~30 min of visible light irradiation, the decomposition ratio of RhB is up to ~97.4%. The excellent photocatalytic performance of $ZnFe_2O_4$ photocatalyst is attributed to the high effective oxidation–reduction reaction caused by light irradiation excitation. With the increase of decomposition time, the wavelength of the maximum absorption peak of RhB solutions shifts from 557 nm to 498 nm ("blue shift"), which is because of the N-deethylation and cleavage of the conjugated chromophore structure of RhB. $ZnFe_2O_4$ photocatalyst also exhibits a weak ferromagnetism performance. The decomposition ratio of RhB for the magnetically recycled $ZnFe_2O_4$ is ~94.6%. Strong visible light photocatalysis and convenience of magnetic recycling make $ZnFe_2O_4$ promising for photocatalytic applications in dye wastewater treatment.

Key words: Electroceramics, sol–gel method, oxides, magnetic zinc ferrite, visible light photocatalyst

INTRODUCTION

With environmental protection requirements, decomposition of textile industrial dye wastewater has been a hot research topic recently.[1,2] Research on wastewater treatment include biological treatments, physical methods and chemical methods.[3,4] Among these methods, photocatalysis, utilizing the most common energy of nature, with its unique advantages of clean sanitation and safety facilities, has been widely studied.[5,6] Photocatalysis is a process in which light is used to activate a substance, the photocatalyst, which modifies the rate of a chemical reaction without being involved itself in chemical transformation. In 1972, A. Fujishima found the n-type TiO_2 electrode could split water into hydrogen and oxygen via a photoelectrocatalytic process,[7] which aroused an upsurge of researches on traditional semiconductor photocatalytic materials. Vommercial photocatalysts such as ZnO and TiO_2, because of their large gap band (~3.37 eV of ZnO,[8] 3.20–3.56 eV of anatase TiO_2 and 3.00–3.34 eV of rutile TiO_2[9]), only respond to ultraviolet (UV) light.[10,11] It's well-known that visible light accounts for ~46% while UV light only accounts for ~4% of sunlight.[12,13] Therefore, it is urgent to develop visible light photocatalytic materials to utilize solar energy efficiently.

Recently, semiconductors with a narrower band gap have received much more consideration for making full use of solar light. At room temperature, many ferrite materials such as $CaFe_2O_4$ and $MgFe_2O_4$ can effectively utilize visible light due to their smaller band gaps.[14,15] Meanwhile, ferrites are often valued as soft-magnetic materials, because they combine good high-frequency dielectric properties with ferrimagnetic order,[16] giving them the

(Received May 16, 2017; accepted September 13, 2017; published online September 26, 2017)

additional advantage of magnetic separation and reutilization after photocatalytic reaction. Magnetic recycling of photocatalysts provides a convenient and effective way to separate and recycle photocatalysts from solution. Meanwhile, the loss of catalysts during the magnetic recycling process is very low.[17,18] Magnetic $ZnFe_2O_4$ material, possessing a small band gap of ~1.9 eV,[19,20] was selected as a visible light magnetic photocatalyst candidate.

Various approaches have been reported to synthesize $ZnFe_2O_4$ powder, including ball milling,[21] co-precipitation,[22] combustion synthesis[23] and sol–gel methods.[24] Among these methods, the sol–gel method is particularly advantageous due to it being cost-efficient, having control of the purity, uniformity and reliable low-temperature condition requirements for the preparation of nano-ferrites.[25–27]

In this work, ferrite $ZnFe_2O_4$ photocatalyst was synthesized via the sol–gel method, and its strong visible light photocatalytic performance was characterized in detail. Meanwhile, the $ZnFe_2O_4$ nanoparticles were recycled for a secondary decomposition of RhB solutions.

MATERIALS AND METHODS

Starting Materials

All the starting materials were analytical grade. Zinc nitrate hexahydrate [$Zn(NO_3)_2{\cdot}6H_2O$], iron nitrate nonahydrate [$Fe(NO_3)_3{\cdot}9H_2O$], citric acids[$(HOOCCH_2C(OH)(COOH)CH_2COOH$], ammonia water ($NH_4OH$) and RhB were purchased from Sinopharm Chemical Reagent Co., Ltd. Deionized water was employed throughout all experiments.

Preparation of Zinc Ferrite

$Zn(NO_3)_2{\cdot}6H_2O$ and $Fe(NO_3)_3{\cdot}9H_2O$ at a molar ratio of 1:2 were added to 12.5 ml of deionized water. After being dissolved thoroughly, 30 mmol citric acid was added into the solution and stirred for half an hour. The initial pH of the solution was noted as ~1 and adjusted to ~5 by adding ammonia water. The mixture was constantly stirred with the help of magnetic stirrer for about half an hour at 80°C to obtain sol. Then, the sample was transferred to a 120°C air drying oven (HK-350A+, China) for 2 days and annealed at 600°C, then a muffle furnace (SG-XL1100, China) for 2 h. After annealing, the sample was ball-milled into powder before characterization.

Characterizations

The crystalline structure of the synthesized $ZnFe_2O_4$ powder was characterized at room temperature on an x-ray diffractometer (Philips PW3040/60, The Netherlands) using monochromatic Cu Kα radiation (λ = 1.5406 Å, 2θ = 20°–70°). The morphology of the synthesized $ZnFe_2O_4$ powder was characterized on a transmission electron microscope (Hitachi H-7650, Japan). the ferromagnetic loop of $ZnFe_2O_4$ powder was measured via a vibrating sample magnetometer (VSM; LakeShore 7400, USA).

The distilled water solution of RhB (10 mg/L) was chosen for photodecomposition. Time-dependent photodecomposition was studied. 50 mL of RhB solution and 1.5 μL of H_2O_2 were put into a 100-mL glass beaker, together with 1.5 mg/L of $ZnFe_2O_4$ powder. After being activated by Fe(II)/Fe(III), H_2O_2 can produce strong oxidizing hydroxyl (•OH) radicals to promote the reaction due to the well-known heterogeneous Fenton process.[28–30] A 500-W xenon lamp as an illuminant was located above the beaker. A 3-ml sample was taken from the solution every 5 min during a visible light irradiation time of 30 min, and centrifuged at 6000 rpm min^{-1} for 10 min in order to separate the catalyst particles from the solution (H1650 desktop centrifuge, China) before absorption measurement. A Hitachi U-3900 UV–vis spectrophotometer was employed to monitor the change of the absorption spectrum of the RhB solutions after photocatalytic decomposition.

RESULTS AND DISCUSSION

X-ray diffraction (XRD) patterns of calcined $ZnFe_2O_4$ powder are shown in Fig. 1. The characteristic peaks at 30.0°, 35.3°, 36.9°, 42.8°, 53.1°, 56.6°, and 62.2° in the XRD spectra correspond to the characteristic planes (220), (311), (222), (400), (422), (511) and (440) of $ZnFe_2O_4$ powder (JCPDS card no. 22-1012), respectively. No other characteristic peaks of impurities are detected in the diffractogram.

The transmission electron microscope (TEM) image of $ZnFe_2O_4$ is presented in Fig. 2. The average diameter of the $ZnFe_2O_4$ powder is approximately 250 nm. In theory, the photocatalytic decomposition ratio may be obviously influenced by the shape and size of catalysts.[31] Nanocatalysts with high surface area and small size can promote

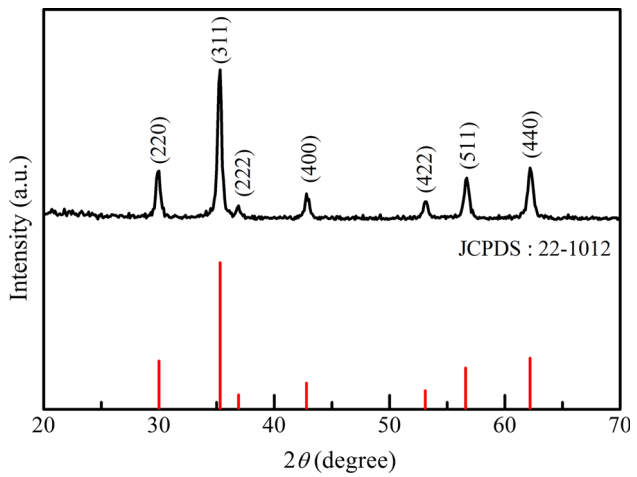

Fig. 1. The XRD pattern of sol–gel-synthesized $ZnFe_2O_4$ powder.

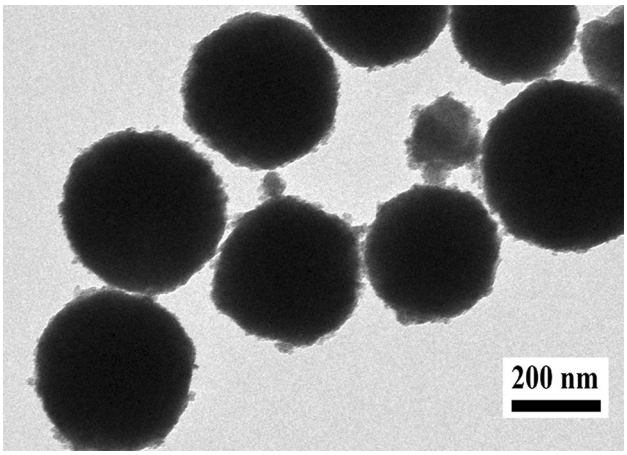

Fig. 2. TEM photograph of $ZnFe_2O_4$.

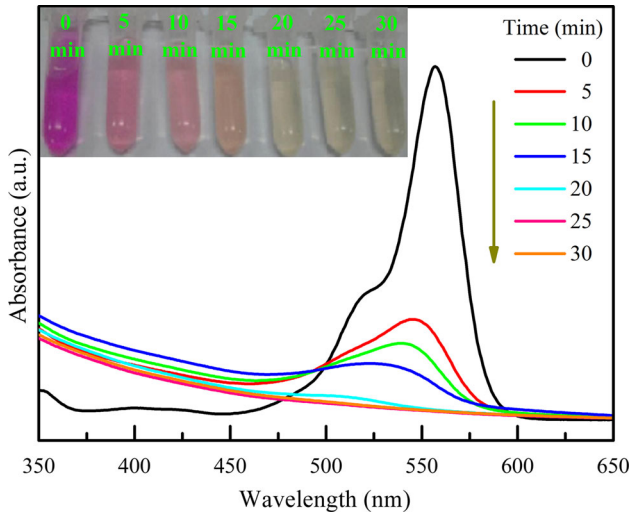

Fig. 3. The adsorption spectra of RhB solution in the presence of $ZnFe_2O_4$ photocatalyst under different visible light irradiation time. The inset photograph shows the color change of RhB.

quick electric charge migration between organic pollutants and catalyst, which results in high decomposition efficiency. However, the small size may also result in a decrease in magnetization value of $ZnFe_2O_4$[32] which is unfavorable for magnetic recycling of photocatalyst.

Figure 3 plots the adsorption spectra of under different irradiation times in the presence of 1.5 g/L $ZnFe_2O_4$. The intensity of the maximum absorption peak of RhB solution weakens rapidly in 25 min, indicating a rapid decomposition of RhB solution. The direct results of decomposition can be found from the inset of Fig. 3. Besides, it is found that the wavelength of maximum absorption peak of RhB solution decreases with the increase of light irradiation time.

A possible mechanism of the photocatalytic decomposition of RhB with $ZnFe_2O_4$ photocatalyst is shown in Fig. 4. The photocatalytic performance can be explained by energy band theory. The electrons in a full valence band (VB) of $ZnFe_2O_4$ will be excited to the empty conduction band (CB) separately under solar light irradiation, leaving an equal number of holes (h^+) with positive charge in corresponding positions. Afterward, the generated electrons (e^-) will act with O_2 to yield superoxide radical anion $\bullet O_2^-$ and the formed $\bullet O_2^-$ ions will further react with H_2O, producing hydroxyl radical $\bullet$OH, which possess strong oxidation ability and can destroy dye molecules completely.[33–35] The mechanism can be proposed as the following formulas:

$$ZnFe_2O_4 \xrightarrow{hv} h^+ + e^- \quad (1)$$

$$e^- + O_2 \rightarrow \bullet O_2^- \quad (2)$$

$$\bullet O_2^- + H_2O \rightarrow \bullet HO_2 + OH^- \quad (3)$$

$$\bullet HO_2 + H_2O \rightarrow H_2O_2 + \bullet OH \quad (4)$$

$$H_2O_2 \rightarrow 2 \bullet OH \quad (5)$$

$$h^+ + OH^- \rightarrow \bullet OH \quad (6)$$

$$2 \bullet OH + \text{dye} \rightarrow H_2O + CO_2 \quad (7)$$

Figure 5 shows the extract information of Fig. 3, including the irradiation time dependence on decomposition ratio and the wavelength of the maximum absorption peak of RhB solutions. The decomposition ratio of RhB solutions is close to 73.1% in 5 min and 97.4% in 25 min. Meanwhile, the wavelength of the maximum adsorption peak decreases from 557 to 498 nm considerably throughout the irradiation time, which is called “blue shift”. Based on the N-deethylation mechanism, decomposition of RhB solutions can be explained as N-deethylation and cleavage of the conjugated chromophore structure.[36] The RhB molecule underwent efficient N-deethylation under visible light irradiation so that the the wavelength of the maximum adsorption peak decreased. Cleavage of the conjugated chromophore structure of RhB led to the bleaching of the dye.[37–40] From experimental results shown in Fig. 3, it can be found that both processes occurred simultaneously in the photocatalytic decomposition process.

Figure 6 shows the adsorption spectra of 10 mg/L RhB solution under a visible light irradiation time of 25 min in the presence of different $ZnFe_2O_4$ mass concentrations of 0–3.5 g/L. The inset of Fig. 6 plots the dependence of the mass concentration of $ZnFe_2O_4$ on the decomposition ratio of RhB solution. In Fig. 6, with the increase of the mass concentration of $ZnFe_2O_4$, the decomposition ratio of RhB exhibits a gradual increase first, and thereafter shows a slight decreasing trend. The optimal photocatalytic decomposition occurs for ~1.5 g/L $ZnFe_2O_4$ photocatalyst. This result may be explained as following: First, since

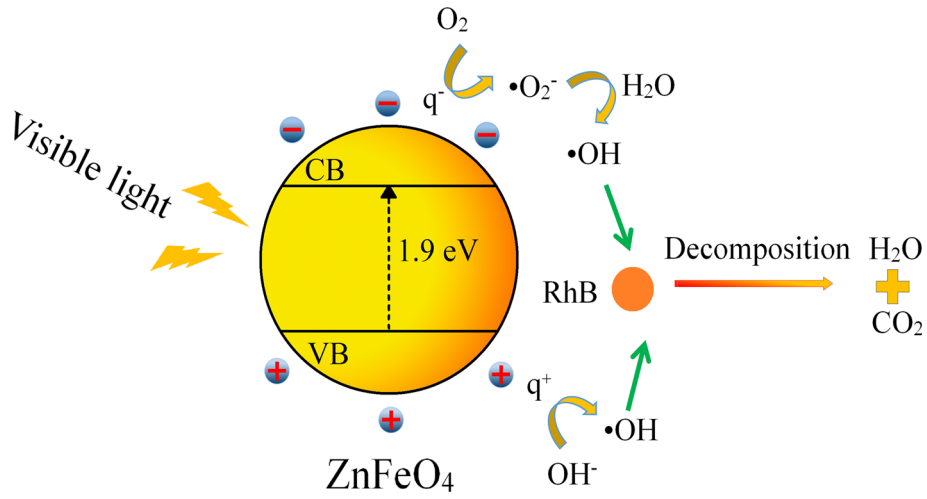

Fig. 4. Mechanism of the photocatalytic decomposition of RhB with $ZnFe_2O_4$ photocatalyst.

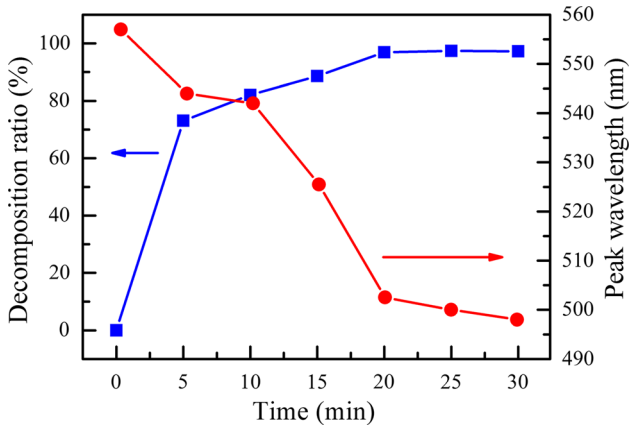

Fig. 5. The visible light irradiation time dependence on the decomposition ratio and the peak wavelength of RhB wastewater solution.

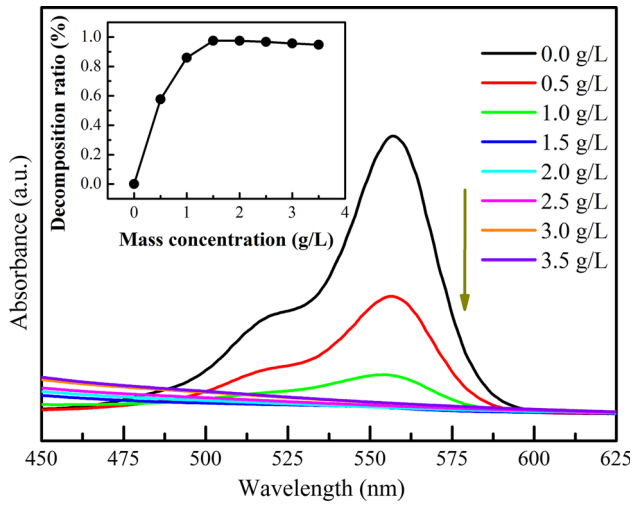

Fig. 6. The adsorption spectra of RhB solution under a visible light irradiation time of 25 min in the presence of different mass concentrations of $ZnFe_2O_4$ photocatalyst. The inset plots the dependence of the mass concentration on the decomposition ratio of RhB solution.

the lifetime of the photocatalytically induced oxidizing species is extremely short (only a few nanoseconds), the photocatalytic reaction only occurs around the generated active species. A high mass concentration of $ZnFe_2O_4$ can enhance the probability of collision between these active species and dye molecules, which can help to increase the decomposition ratio.[41] When the mass concentration of $ZnFe_2O_4$ continues to increase and exceeds 1.5 g/L, the decomposition ratio of RhB decreases slightly because of recombination and quenching of the photo-induced electron–hole pairs.[42] What's more, the excess $ZnFe_2O_4$ photocatalyst in wastewater solution will also decrease the transmissivity of visible light and strengthen the scattering effect on light irradiation,[43] leading to the slight decrease of decomposition ratio for excessive catalyst in Fig. 6.

Figure 7 shows the ferromagnetic loop of $ZnFe_2O_4$ powder. As shown in Fig. 7, the ferrite $ZnFe_2O_4$ material displays weak ferromagnetism performance at room temperature, which is favorable for the magnetic recycling of the photocatalyst.

In order to investigate the stability and reusability of $ZnFe_2O_4$ catalyst, $ZnFe_2O_4$ catalyst was subjected to a cyclic decomposition experiment. Figure 8 plots the visible light irradiation time dependence on the decomposition ratio of 10 mg/L RhB solution for the magnetically recycled $ZnFe_2O_4$ photocatalyst. The inset of Fig. 8 shows the separation picture of $ZnFe_2O_4$ photocatalyst from wastewater solution under the magnetic field of a magnet.[44,45] After finishing photocatalysis, $ZnFe_2O_4$ catalyst uniformly dispersed in RhB dye solution as shown in inset (a) of Fig. 8. Under the magnetic field of a magnet, $ZnFe_2O_4$ powders were easily magnetically harvested with a ~94.8% recycling rate (defined as the ratio of the initial catalysts mass to the recycling catalyst mass). After separation, the almost transparent wastewater solution

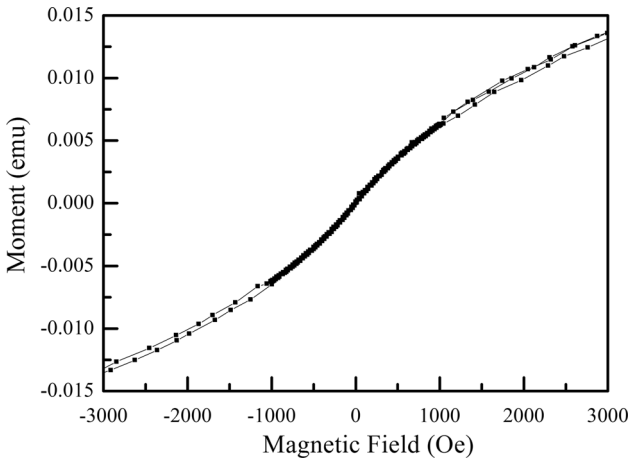

Fig. 7. The ferromagnetic characterization of $ZnFe_2O_4$ powder.

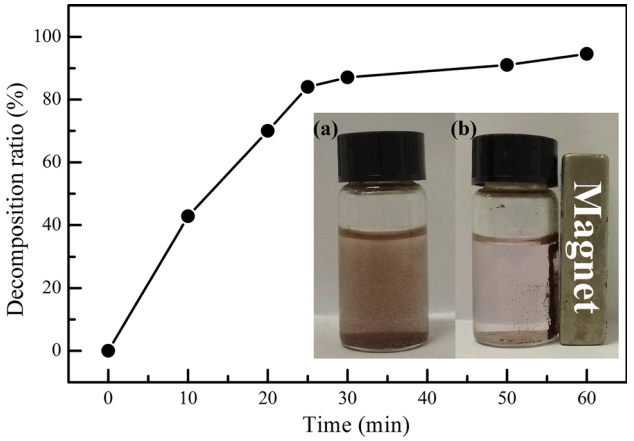

Fig. 8. The visible light irradiation time dependence on the decomposition ratio after magnetically recycling $ZnFe_2O_4$ photocatalyst. The inset is a picture of $ZnFe_2O_4$ photocatalyst separating from wastewater solution under a magnetic field.

was obtained as shown in inset (b) of Fig. 8. In Fig. 8, the measured decomposition ratio for the magnetically recycled $ZnFe_2O_4$ photocatalyst is up to ~94.6%. These advantages of strong visible light photocatalytic performance and magnetically recyclable performance make $ZnFe_2O_4$ catalyst materials promising in dye wastewater photocatalytic treatment.

CONCLUSIONS

In summary, a magnetically separable $ZnFe_2O_4$ photocatalyst was synthesized via a sol–gel method. $ZnFe_2O_4$ photocatalyst displays excellent photocatalytic activity for decomposing RhB solution with a high decomposition ratio of ~97.4%. After magnetically recycling $ZnFe_2O_4$ catalysts, the decomposition ratio is still up to ~94.6%. The excellent visible light photocatalysis and convenience of magnetic recycling make $ZnFe_2O_4$ a potential candidate for application in dealing with dye wastewater.

ACKNOWLEDGEMENTS

This work was supported by the National Natural Science Foundation of China (No. 51502266) and the Public Welfare Technology Application Research Project of Zhejiang Province, China (LGG18E020005).

REFERENCES

1. M. Sundararajan, L.J. Kennedy, P. Nithya, J.J. Vijaya, and M. Bououdina, *J. Phys. Chem. Solids* 108, 61 (2017).
2. H. You, Y. Jia, Z. Wu, X. Xu, W. Qian, Y. Xia, and M. Ismail, *Electrochem. Commun.* 79, 55 (2017).
3. G. Crini, *Bioresour. Technol.* 97, 1061 (2006).
4. Y. Xia, Y. Jia, W. Qian, X. Xu, Z. Wu, Z. Han, Y. Hong, H. You, M. Ismail, G. Bai, and L. Wang, *Metals* 7, 122 (2017).
5. U.I. Gayaa and A.H. Abdullah, *J. Photochem. Photobiol. C* 9, 1 (2008).
6. S. Malato, P. Fernández-Ibáñez, M.I. Maldonado, J. Blanco, and W. Gernjak, *Catal. Today* 147, 1 (2009).
7. A. Fujishima, *Nature* 238, 37 (1972).
8. D.M. Bagnall, Y.F. Chen, Z. Zhu, T. Yao, S. Koyama, M.Y. Shen, and T. Goto, *Appl. Phys. Lett.* 70, 2230 (1997).
9. A. Nakaruk, D. Ragazzon, and C.C. Sorrell, *Thin Solid Films* 518, 3735 (2010).
10. S. Rehman, R. Ullah, A.M. Butt, and N.D. Gohar, *J. Hazard. Mater.* 170, 560 (2009).
11. M.R. Hoffman, S.T. Martin, W.Y. Choi, and D.W. Bahnemann, *Chem. Rev.* 95, 69 (1995).
12. X. Chen, S. Shen, L. Guo, and S.S. Mao, *Chem. Rev.* 110, 6503 (2010).
13. S. Li, Y. Lin, B. Zhang, C. Nan, and Y. Wang, *J. Appl. Phys.* 105, 056105 (2009).
14. S. Ida, K. Yamada, T. Matsunaga, H. Hagiwara, Y. Matsumoto, and T. Ishihara, *J. Am. Chem. Soc.* 132, 17343 (2010).
15. R. Dom, R. Subasri, K. Radha, and P.H. Borse, *Solid State Commun.* 151, 470 (2011).
16. Y. Jia, H. Luo, S. Or, Y. Wang, and H.L.W. Chan, *J. Appl. Phys.* 105, 124109 (2009).
17. C. Tan, G. Zhu, M. Hojamberdiev, C. Xu, J. Liang, P. Luo, and Y. Liu, *J. Clust. Sci.* 24, 1115 (2013).
18. B. Tian, T. Wang, R. Dong, S. Bao, F. Yang, and J. Zhang, *Appl. Catal. B* 147, 22 (2014).
19. X. Li, Y. Hou, Q. Zhao, W. Teng, X. Hu, and G. Chen, *Chemosphere* 82, 581 (2011).
20. X. Xu, Z. Wu, Y. Jia, W. Li, Y. Liu, Y. Zhang, and A. Xue, *J. Nanomater.* 2015, 613565 (2015).
21. M. Jean and V. Nachbaur, *J. Alloys Compd.* 454, 432 (2008).
22. A.S. Singh, U.B. Patil, and J.M. Nagarkar, *Catal. Commun.* 35, 11 (2013).
23. A. Manikandan, L.J. Kennedy, M. Bououdina, and J.J. Vijaya, *J. Magn. Magn. Mater.* 349, 249 (2014).
24. S.A. Oliver, *Phys. Rev. B* 60, 3400 (1999).
25. S.E. Shirsath, B.G. Toksha, R.H. Kadam, S.M. Patange, D.R. Mane, G.S. Jangam, and A. Ghasemi, *J. Phys. Chem. Solids* 71, 1669 (2010).
26. Y. Jia, Z. Zhou, Y. Wei, Z. Wu, J. Chen, Y. Zhang, and Y. Liu, *J. Appl. Phys.* 114, 213903 (2013).
27. Y. Jia, Z. Zhou, Y. Wei, Z. Wu, H. Wang, J. Chen, Y. Zhang, and Y. Liu, *Smart Mater. Struct.* 22, 125014 (2013).
28. G. Centi, S. Perathoner, T. Torre, and M.G. Verduna, *Catal. Today* 55, 61 (2000).
29. S. Sun, W. Wang, L. Zhong, and M. Shang, *J. Phys. Chem. C* 113, 12826 (2009).
30. W. Luo, L. Zhu, N. Wang, H. Tang, M. Cao, and Y. She, *Environ. Sci. Techonol.* 44, 1786 (2010).
31. Y.F. Li and Z.P. Liu, *J. Am. Chem. Soc.* 133, 15743 (2011).
32. A. Shanmugavani, R. Kalai Selvan, S. Layek, and C. Sanjeeviraja, *J. Magn. Magn. Mater.* 354, 363 (2014).
33. W. Qian, Z. Wu, Y. Jia, Y. Hong, X. Xu, H. You, Y. Zheng, and Y. Xia, *Electrochem. Commun.* 81, 124 (2017).
34. J. Wu, W. Mao, Z. Wu, X. Xu, H. You, A. Xue, and Y. Jia, *Nanoscale* 8, 7343 (2016).

35. H. Lin, Z. Wu, Y. Jia, W. Li, R. Zheng, and H. Luo, *Appl. Phys. Lett.* 104, 162907 (2014).
36. S. Horikoshi, A. Saitou, H. Hidaka, and N. Serpone, *Environ. Sci. Technol.* 37, 5813 (2003).
37. Q. Wang, C. Chen, D. Zhao, W. Ma, and J. Zhao, *Langmuir* 24, 7338 (2008).
38. H. Park and W. Choi, *J. Phys. Chem. B* 109, 11667 (2005).
39. X. Hu, T. Mohamood, W. Ma, C. Chen, and J. Zhao, *J. Phys. Chem. B* 110, 26012 (2006).
40. C. Chen, W. Zhao, P. Lei, J. Zhao, and N. Serpone, *Chem Eur. J.* 10, 1956 (2004).
41. N. Barka, S. Qourzal, A. Assabbane, A. Nounah, and Y. Ait-Ichou, *J. Photochem. Photobiol. A* 195, 346 (2008).
42. H. You, Z. Wu, Y. Jia, X. Xu, Y. Xia, Z. Han, and Y. Wang, *Chemosphere* 183, 528 (2017).
43. P. Chen, Y. Zhang, F. Zhao, H. Gao, X. Chen, and Z. An, *Mater. Charact.* 114, 243 (2016).
44. M. Shokouhimehr, Y. Piao, J. Kim, Y. Jang, and T. Hyeon, *Angew. Chem. Int. Ed.* 46, 7039 (2007).
45. M. Wang, Y. Ma, X. Sun, B. Geng, M. Wu, G. Zheng, and Z. Dai, *Appl. Surf. Sci.* 392, 1078 (2017).